Applied Energy 113 (2014) 515–523

Contents lists available at ScienceDirect

Applied Energy

journal homepage: www.elsevier.com/locate/apenergy

Mineral carbonation from metal wastes: Effect of solid to liquid ratio on the efficiency and characterization of carbonated products ☆

Marco Dri, Aimaro Sanna, M. Mercedes Maroto-Valer *

Centre for Innovation in Carbon Capture and Storage (CICCS), School of Engineering and Physical Sciences, Heriot-Watt University, Edinburgh EH14 4AS, UK

HIGHLIGHTS

- Steel, phosphorus and blast furnace slags are suitable feedstock for mineralization.
- Efficiency of carbonation increases for all 3 materials when S/L ratio decreases.
- Silica from the raw material did not dissolve and formed the core of final particles.
- $CaSO_4$ left from incomplete carbonation also formed the core of final particles.
- $CaCO_3$ was deposited on the surface of the carbonated final particles.

ARTICLE INFO

Article history:
Received 1 April 2013
Received in revised form 3 July 2013
Accepted 29 July 2013
Available online 24 August 2013

Keywords:
CCS
Mineral carbonation
Multi-step process
Metal waste materials

ABSTRACT

Mineral carbonation technologies aim at permanently storing CO_2 into materials rich in metal oxides. A multi-step mineralization process employing Ca-rich waste streams to precipitate calcium carbonate is investigated in this paper. Ground granulated blast furnace slag (GGBS), phosphorus slag (PS) and steel slag (SS) were employed as feeding materials for the process. Solid to liquid ratio (S/L) is an important factor which affects mineral carbonation and this study examines its effect on the carbonation efficiencies. The main phases present in the carbonated residues were identified using XRF, XRD and SEM–EDS analytical techniques. For the three materials investigated, the carbonation efficiency increased when the S/L ratio decreased (from 50 g/L to 25 g/L and then 15 g/L) because of the dilution effect. In a previous study, where an analog process was employed, efficiency using serpentine was found lower than that calculated here for GGBS and SS, and slightly above PS. This confirms that, in general, waste materials require less energy-intensive carbonation conditions, in comparison to mineral rocks. Finally, the structure of the carbonated particles is also discussed.

1. Introduction

Nowadays fossil fuels account for 80–85% of the total of world energy use and they cause the release of about 30 Gt/year of CO_2 into the atmosphere [1]. Considering that CO_2 is a greenhouse gas, such large and increasing atmospheric CO_2 levels are causing climatic consequences [2]. In fact, it has been shown that the global average air and ocean temperatures have been increasing, global sea levels raising [3] and the number of severe weather events intensifying [4].

Carbon dioxide capture and storage (CCS) is a portfolio of technologies aiming to capture the CO_2 produced from the combustion of fossil fuels and other energy intensive process and then store it underground for a very long time [5]. Recently, interest for an alternative route to geological storage, called mineral carbonation or mineralization, has increased because of its advantages of vast and permanent storage capacity [6]. The mineralization process consists of reacting CO_2 with a divalent metal oxide (MO) to produce a metal carbonate (MCO_3). However, despite the intrinsic advantages of mineralization, including being an ex-situ and permanent process, its costs are currently considered not competitive compared to those of geological storage [7].

At ambient conditions, the gas–solid mineralization reaction takes place on geological time-scales and, therefore, research has focused on developing different technologies to speed up the process [2]. A closed-loop, multi-step process using ammonium salts has recently been developed to extract magnesium from serpentine and produce separated streams of pure by-products at ambient pressure [6,8]. Furthermore, this process allows recovery of the chemicals used, reducing the overall environmental and economical impact, but thus far it has only been applied to serpentine minerals. It is interesting to highlight that there is increasing interest in using alkaline industrial waste residues as feedstock material

* Corresponding author. Tel.: +44 (0) 131 451 8028.
E-mail address: m.maroto-valer@hw.ac.uk (M.M. Maroto-Valer).

0306-2619/$ - see front matter © 2013 The Authors. Published by Elsevier Ltd. All rights reserved.
http://dx.doi.org/10.1016/j.apenergy.2013.07.064

for mineral carbonation [9–13]. This is because these materials require a lower degree of pre-treatment and less energy-intensive carbonation conditions, in comparison to mineral rocks [14,15]. Moreover, waste materials have the potential of storing 1 Mt/year CO_2 in the UK alone [16] and, furthermore, their use would avoid disposal requirements and could transform them into a potential revenue resource instead of a costly waste stream. However, their storage potential is limited if compared to the annual CO_2 emissions in the UK (470 Mt) [17]. This technology could be attractive for cases where the producer of suitable waste materials and the CO_2 emitter are located in close proximity [16].

This paper focuses on using a process similar to that previously developed for magnesium-rich serpentine minerals by Wang and Maroto-Valer [6,8], but employing calcium-rich waste streams, and therefore resulting in the precipitation of calcium carbonate instead of magnesium carbonate. The proposed mineralization process includes four main steps (Fig. 1): (1) mineral dissolution, (2) pH adjustment and precipitation of impurities, (3) carbonation reaction, and (4) regeneration of additives.

The overall process utilizes ammonium bisulfate (NH_4HSO_4) solution for the mineral dissolution phase (step 1), extracting calcium from the waste feeding materials and producing solid calcium sulfate ($CaSO_4$). This is an intrinsic difference with the process developed for serpentine, where, following the mineral dissolution step, $MgSO_4$ is formed in solution, while here $CaSO_4$ is precipitated. In fact, the two sulfates have different values of solubility in water, $CaSO_4$ has been reported of being slightly soluble [18] while $MgSO_4$ has a solubility of 26 g/100 mL (20 °C) [19]. Afterwards, ammonium carbonate ($(NH_4)_2CO_3$), from the CO_2 capture step, is added in the carbonation step (step 3), allowing the precipitation of calcium carbonate ($CaCO_3$). Raising the pH (step 2) is an important step between dissolution and carbonation because it allows the following precipitation of $CaCO_3$. While the pH is raised, the impurities (Mg, Fe, Al) precipitate as hydroxides. This carbonation process could also re-circulate and regenerate the chemicals involved (step 4), i.e. NH_4HSO_4 and NH_3. Therefore, this paper investigates the process described above for three different metal wastes: ground granulated blast furnace slag (GGBS), phosphorus slag (PS) and steel slag (SS). For each waste material, the dissolution, adjustment of pH and carbonation steps of the overall close-loop mineralization process were studied.

Furthermore, solid-to-liquid (S/L) ratio is an important parameter which has been shown to affect significantly the efficiency of mineralization of serpentines [9,20,21,22,23]. Therefore, this work also investigates the effect of three different S/L ratios, starting from 50 g/L, the same employed by Wang and Maroto-Valer [6], and then reducing to 25 and 15 g/L in an attempt to improve the efficiency of mineralization, as previously reported for coal fly ash and steel slag [22] [24].

2. Experimental methods

2.1. Characterization of the parent samples

The three feedstock materials, namely, SS, GGBS and PS employed for this study were obtained from production plants of steel, iron and phosphorus respectively where a representative amount of 5 kg of each sample was collected from the residue of the manufacturing process and safely stored indoor for the experiments. SS is the by-product of the manufacture of steel from pig iron (blast furnace) and metal scrap and it was obtained from an electric arc furnace. GGBS is a by-product from the production of iron, resulting from the fusion of fluxing stone (fluorspar) with coke, ash and the siliceous and aluminous residues remaining after the reduction and separation of iron from the ore. PS is the by-product from yellow phosphorus production obtained from electric furnaces.

SS, GGBS and PS were characterized employing different techniques to assess the parameters important for mineral carbonation. The loss on ignition (LOI) was determined gravimetrically by taking ~1 g of a crushed representative sample from each material and drying for 1 h at 950 °C. Oxide composition was characterized using a PANalytical Axios Advanced X-ray Fluorescence (XRF) spectrometer. For XRF analysis, a fused bead sample was prepared using ~1 g of a crushed and finely ground representative sample.

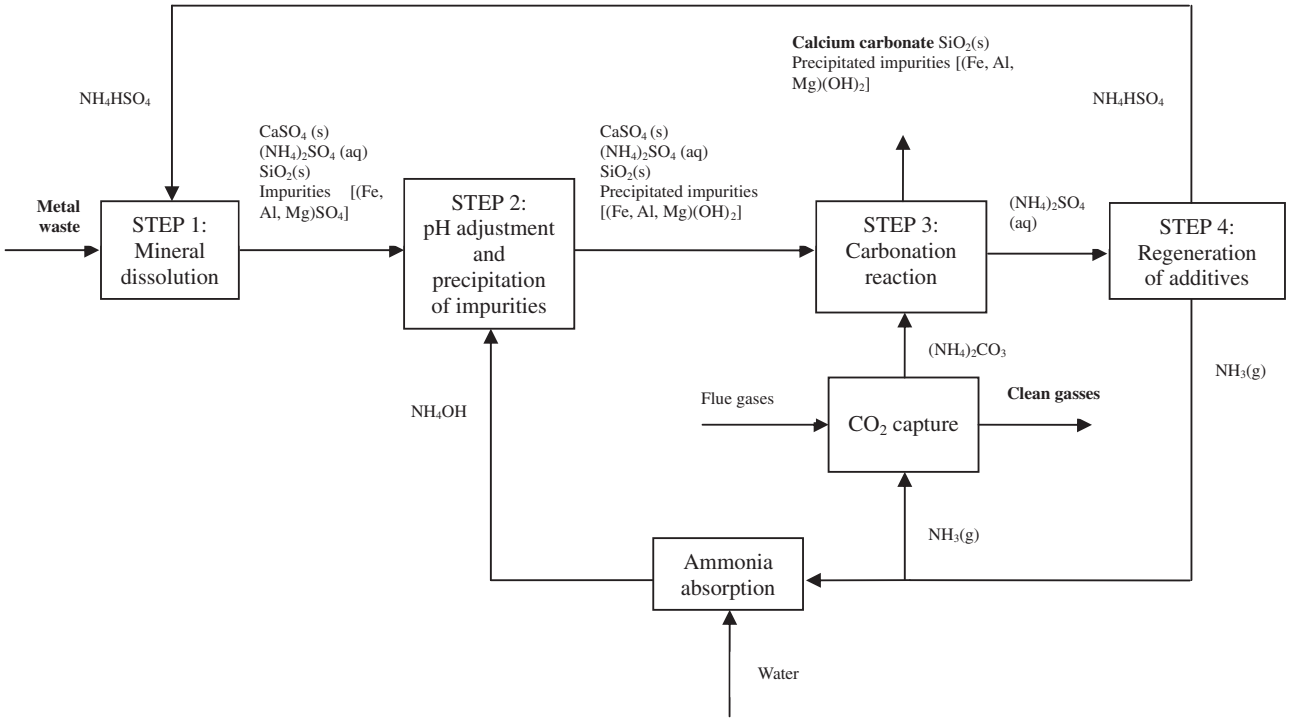

Fig. 1. Multi-step close loop mineral carbonation process.

Characterization of the crystalline mineral phases present in SS, PS and GGBS was achieved using a Hiltonbrooks X-ray Diffractometer (XRD) using a 3 kW generator, scan speed of 2°/min (2θ), and a step size of 0.05 across the range 5–65° (2θ) under 40 kV/40 mA. About 10 g of a crushed representative sample was finely ground and stored in a sample holder for the XRD analysis.

2.2. Dissolution and carbonation experiments

This paper focuses on the dissolution, adjustment of pH and carbonation steps of the overall close-loop mineralization process (Fig. 1).

Following the procedure developed by Wang and Maroto-Valer [6], experiments were carried out in a 500 mL 3 necks glass flask which was heated by a temperature-controlled silicone oil bath and a thermocouple. The solution was continuously mixed by a stirrer and, to avoid evaporation losses, the rig was connected to a water cooling system via one of the necks. Samples were ground and sieved to a particle size fraction of 75–150 μm as in previous studies [6,8].

The solutions employed were prepared with stochiometric NH_4HSO_4 (Table 1) based on (i) the S/L ratio used in the experiments, (ii) the concentration of Ca in the raw materials and (iii) the theoretical dissolution reaction between Ca silicates and NH_4HSO_4:

$$CaO \cdot SiO_2 + 2NH_4SO_4 \rightarrow CaSO_4 + SiO_2 + H_2O + (NH_4)_2SO_4 \quad (1)$$

The carbonation step was also carried out employing stoichiometric $(NH_4)_2CO_3$ (Table 1) based on the amount of $CaSO_4$ obtained from the dissolution step and the theoretical carbonation reaction:

$$CaSO_4 + (NH_4)_2CO_3 \rightarrow CaCO_3 + (NH_4)_2SO_4 \quad (2)$$

According to the analog process developed by Wang and Maroto-Valer [6,8], dissolution experiments were carried out at 50 °C for 3 h. The adjustment of pH and precipitation of impurities steps took place by adding ammonia water (NH_4OH) in the solution, and raising the pH at about 8.2–8.3. The carbonation step was then conducted for 1 h at 65 °C.

2.3. Characterization of the final solid residue

After each of the mineral carbonation experiments, the solution was filtered and the solid residues dried in an oven at 105 °C until constant mass was achieved.

The efficiency of carbonation was calculated as:

$$\xi_{Ca}\% = \frac{\text{Ca mass in } CaCO_3 \text{ (after carbonation)} - \text{Ca mass in } CaCO_3 \text{ (before carbonation)}}{\text{Ca total mass in feeding material}} \times 100 \quad (3)$$

Because the waste streams suitable for mineral carbonation and studied in this paper are rich in CaO, the efficiency of carbonation has been calculated considering only the conversion of CaO into $CaCO_3$, and small contributions from other metals (e.g. Mg, Fe) have not been included. For each final solid residue the Ca mass in $CaCO_3$ before and after experiments was calculated from duplicate thermo-gravimetric analyses (TGA) employing a TA Q500 instrument. Observing the wt% of CO_2 released in the temperature range 600–850 °C [24] the content of $CaCO_3$ can be calculated using the following formula:

$$\text{Ca mass in } CaCO_3 = \text{weight decrease}_{600-850\,^\circ C}\% \times \frac{MW_{Ca}(kg/mol)}{MW_{CO_2}(kg/mol)} \times \text{mass of solid residue} \quad (4)$$

The oxide composition of solid residues for each product was determined using XRF and XRD following the methodology described in Section 2.1. A SEM JEOL JSM-6400 was employed to study the morphology and composition of the particles. Secondary electron (SE) images were collected using 20 kV beam voltage, 15 mm working distance and the chemical microanalyses were performed with a Link ISIS 300 EDX microanalysis system fitted with a Si(Li) detector. SEM analyses required ~1 g representative finely ground samples which were adhered to a carbon tab prior to sputter a coating with platinum at 2.2 kV for 90 s.

3. Results and discussion

3.1. Characterization of the parent samples

XRF studies were conducted on the parent samples to determine the major oxides present and the results are reported in Table 2. High CaO content implies a good predisposition of the materials towards mineral carbonation for the production of calcium carbonate. All three materials also contain a considerable amount of silica and, as expected, SS is rich in iron oxides, as this sample was procured from a steel production plant where iron minerals are one of the main feedstock for the process. Furthermore, GGBS and SS also present Mg oxides that are expected to precipitate during the carbonation step (Fig. 1).

The LOI value for the SS sample is higher than that of the GGBS and PS samples. This can be attributed to the decomposition of $CaCO_3$, as confirmed by the XRD studies below. The inherent Ca content in the parent samples is an important parameter to assess the predisposition of a material for mineral carbonation. However, the mineral phases present are also important, as this will be related to dissolution of Ca from a given mineral phase, and ultimately impact the final carbonation efficiency (See Section 3.3).

Figs. 2a–c show the XRD diffractograms for the three parent samples. SS is characterized by the presence of calcium as oxide (CaO), as well as in silicate form (dicalcium and tricalcium silicates), as previously reported [25]. For the PS sample, calcium is present in silicates together with fluorine as cuspidine and with phosphorus as hydroxylapatite. GGBS is mainly amorphous because of the quenching process in water used during its production. The XRD pattern for SS also shows $CaCO_3$, as expected form the LOI values (Table 2) and this was taken into account in the calculation of the carbonation efficiency, as explained in Section 2.3. The phase Mn_3O_4 matches the peaks at ~18, ~30 and

Table 1
NH_4HSO_4 and $(NH_4)_2CO_3$ concentration used for the dissolution studies based on stoichiometric concentration required, S/L ratio and CaO content.

		NH_4HSO_4 concentration [mol/L]	$(NH_4)_2CO_3$ concentration [mol/L]
SS	15 g/L	0.39	0.20
	25 g/L	0.65	0.32
	50 g/L	1.3	0.65
PS	15 g/L	0.29	0.16
	25 g/L	0.48	0.24
	50 g/L	0.96	0.48
GGBS	15 g/L	0.39	0.20
	25 g/L	0.65	0.32
	50 g/L	1.3	0.65

Table 2
Chemical composition of the studied samples obtained by XRF.

	Chemical composition (wt%)						
	CaO	MgO	Fe_2O_3	Al_2O_3	SiO_2	MnO	LOI
GGBS	38.98	8.73	0.51	12.54	34.61	0.34	0.36
SS	38.44	8.96	22.53	2.74	12.13	3.58	9.00
PS	46.68	1.24	0.83	2.60	43.07	0.06	0.35

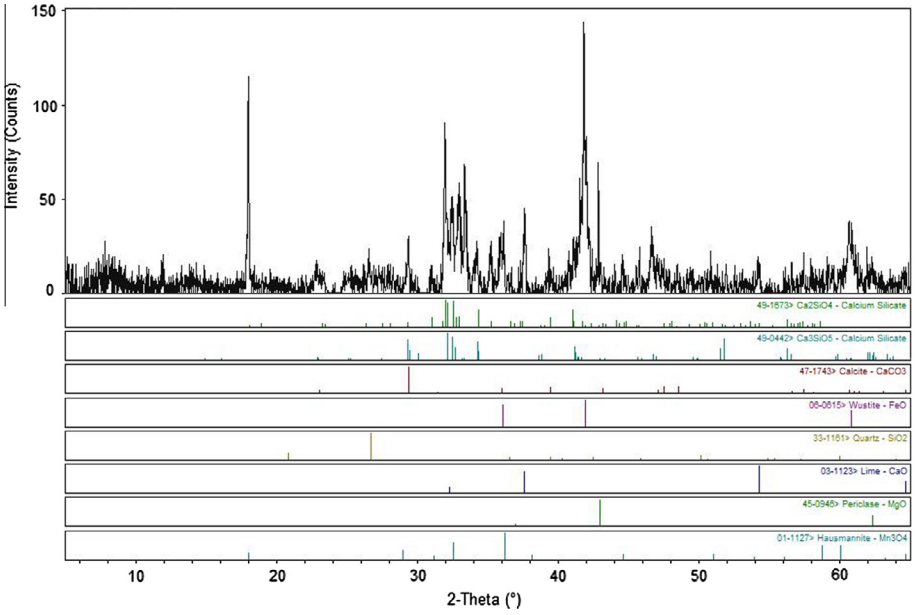

Fig. 2a. XRD diffractogram of SS presenting crystalline phases detected.

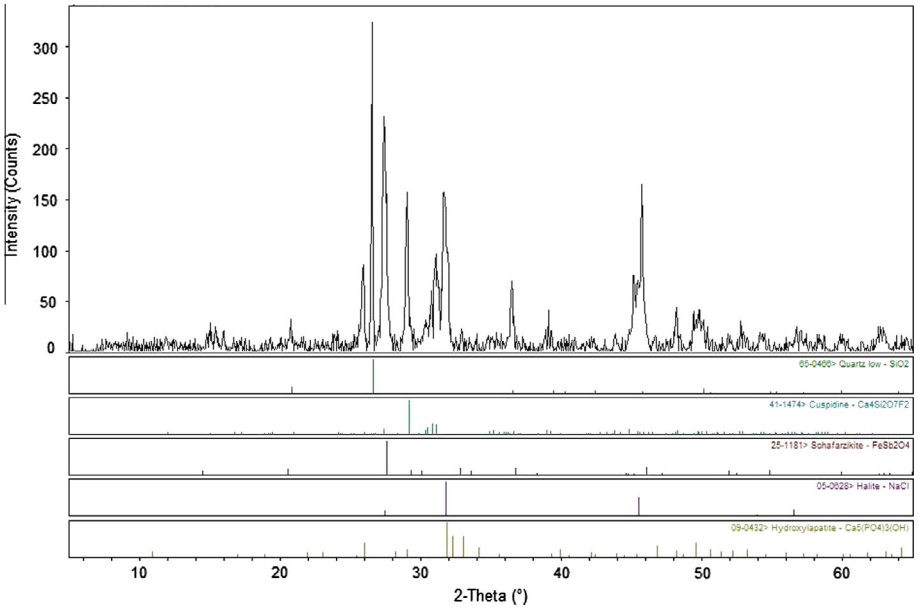

Fig. 2b. XRD diffractogram of PS presenting crystalline phases detected.

~36 2θ degrees of the XRD pattern, confirming its presence in the slag, and the wt% of MnO has been included in the chemical composition reported in Table 2.

3.2. TGA of carbonated residues

TGA tests were carried out on the carbonated solid residues obtained after the experiments on SS, PS and GGBS samples using three different S/L ratios (15–25–50 g/L) and the carbonation efficiencies as a function of the S/L ratio values are presented in Fig. 3. Variations of efficiency amongst experiments on the same feedstock are significant, as the experimental error was estimated to be ±2%, obtained repeating 30% of tests. The maximum efficiencies achieved were for the lowest S/L ratio with values of 74%, 67% and 59% for SS, GGBS and PS, respectively. It can be seen that the carbonation efficiency increases as the S/L ratio decreases, for all three materials, with a slight difference in the trends, as explained below. This variation of the carbonation efficiency with S/L ratio has been reported previously [21,22], where carbonation experiments on coal fly ashes and wollastonite, both Ca-rich feedstock, found increasing levels of efficiency when reducing the S/L ratio. In mineralization multi-step processes, trends of efficiency of carbonation are primarily affected by the Ca extraction conditions during the first phase of the experiments [22]. When reducing the S/L ratio, Ca extraction efficiency improves due to the dilution effect (larger volumes of solution increase the solubility of Ca) [26] and, consequently, also efficiency of carbonation of the multi-step process improves. It should be noted that the carbonation efficiencies of SS are consistently higher than those reported for PS, despite of SS presenting lower initial CaO content than PS

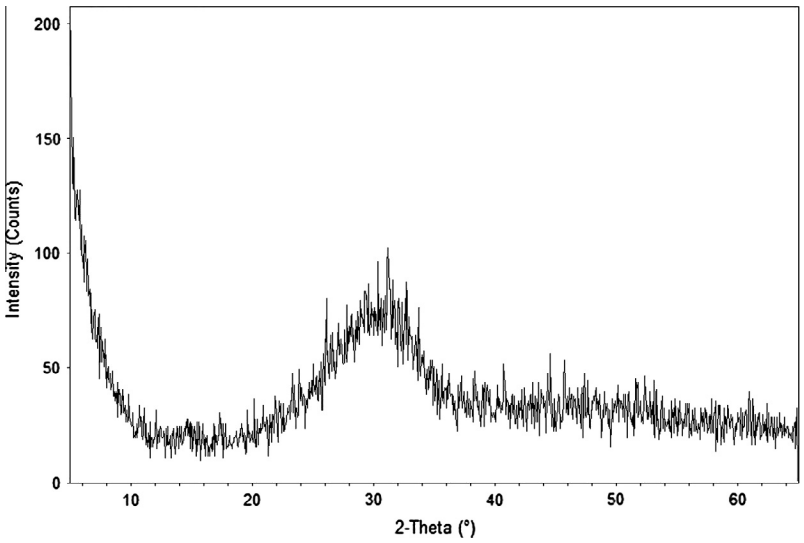

Fig. 2c. XRD diffractogram of GGBS.

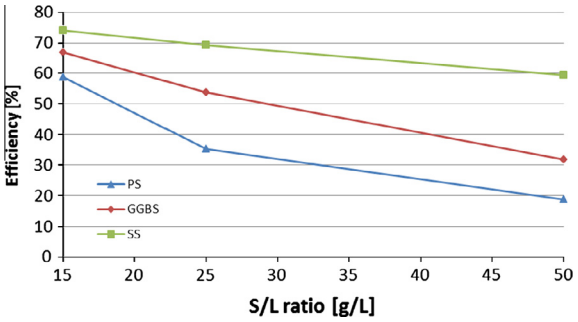

Fig. 3. Efficiencies of carbonation for different S/L ratio values.

(38.44 vs. 46.68, Table 2). This could be related to the different mineral phases present in the parent samples, where extraction of calcium from the mineral phases present in SS (Fig. 2a) seems to be easier than from the mineral phases of PS (Fig. 2b). Relation between mineral phases present in the raw material and efficiency of carbonation could not be investigated for GGBS because of its amorphous nature, as seen in Fig. 2c.

Mineralization of waste materials, in general, requires less energy-intensive carbonation conditions, in comparison to mineral rocks [14,15]. In fact, the carbonation efficiency achieved by the process developed by Wang and Maroto-Valer (similar to the one here employed) using serpentine at 50 g/L was 25% [8] which is lower than that of GGBS and SS, and slightly above that of PS (Fig. 3).

3.3. XRF of carbonated residues

Results from XRF analyses obtained from the carbonated residues are presented in Table 3 (instrumental error ± 0.1%). As expected, these samples present much higher LOI values than their parent samples (Table 2) as they have been carbonated (See Section 3.4 for further discussion of the carbonated products). It can be seen that for the three materials investigated, as soon as the S/L ratio decreases, the SO_3 content diminishes. This is due to the production of calcium carbonate being higher when the S/L ratio is lower (higher carbonation efficiency, Fig. 3) causing lower amounts of residual calcium sulfate left from the dissolution step. Values of Ca, Mg, Fe, Al and Si oxides in the carbonated samples are lower than those reported for the parent samples because of the precipitation of different phases during the step 3 (carbonation reaction) of the process.

3.4. XRD of carbonated residues

The solid residues from the carbonation step were analyzed by XRD and Figs. 4a–c show the XRD diffractograms obtained from the carbonated residues of SS, PS, GGBS after experiments at 15 g/L. For all the samples, the main phases identified were calcium carbonate and residual hydrated calcium sulfate (gypsum). Moreover, the

Table 3
XRF composition of final solid residues after the carbonation step.

		Chemical composition (wt%)						
		CaO	MgO	Fe_2O_3	Al_2O_3	SiO_2	SO_3	LOI
SS	Residue from 15 g/L	26.9	3.6	19.1	1.5	8.8	11.1	24.8
	Residue from 25 g/L	25.9	3.5	18.2	1.4	8.1	14.9	23.8
	Residue from 50 g/L	25.4	4.4	18.3	1.3	8.4	14.9	23.2
PS	Residue from 15 g/L	29.1	0.5	0.2	1.7	27.1	12.8	26.8
	Residue from 25 g/L	28.7	0.5	0.3	1.7	28.4	12.9	25.4
	Residue from 50 g/L	24.9	0.6	0.2	1.4	23.7	15.9	31.6
GGBS	Residue from 15 g/L	22.8	3.8	0.3	7.2	21.7	15.3	27.7
	Residue from 25 g/L	22.6	3.8	0.4	7.8	22.1	15.7	26.5
	Residue from 50 g/L	15.0	2.7	0.2	5.1	14.2	21.7	40.2

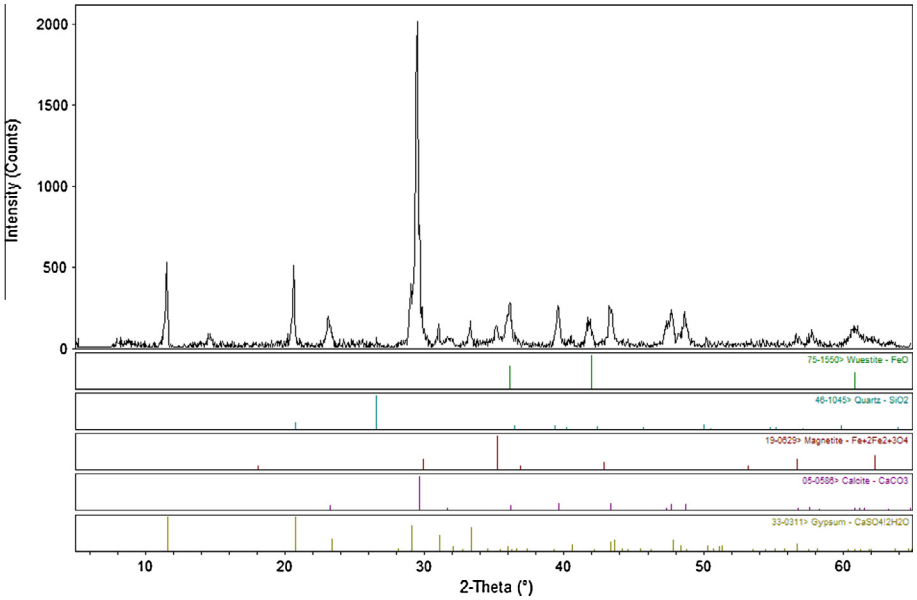

Fig. 4a. XRD diffractogram presenting crystalline phases detected in carbonated SS at 15 g/L.

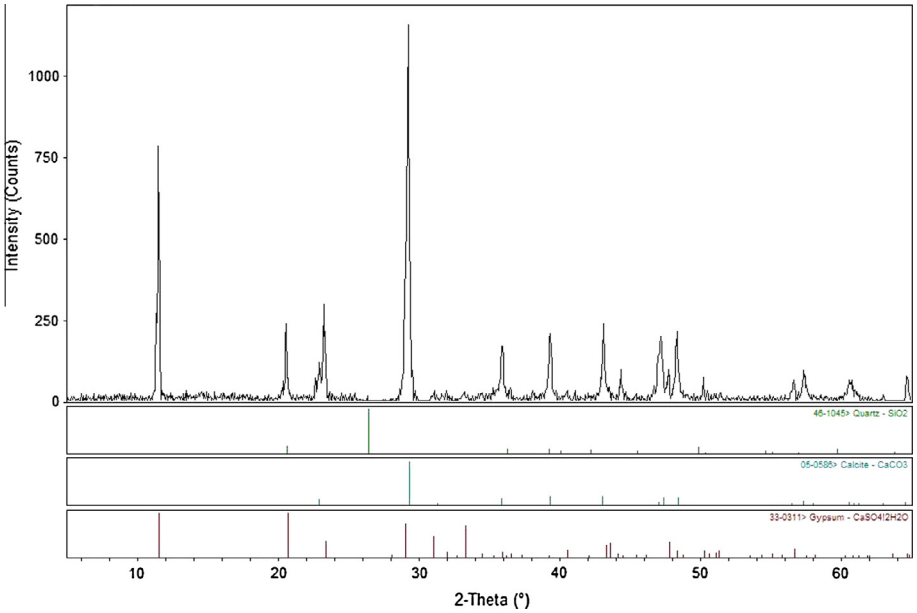

Fig. 4b. XRD diffractogram presenting crystalline phases detected in carbonated PS at 15 g/L.

carbonated SS sample showed also the presence of iron oxide and magnetite (Fig. 4a), as expected form the iron content of the parent samples. Silica peaks (20.5 and 26.5 2θ degrees) were detected as smaller peaks compared to the raw materials in carbonated SS and PS (Fig. 4a and b). This corroborates the values of SiO_2 in Table 3 compared to the values presented in Table 2. SEM studies, confirming the presence of precipitated calcium carbonate and calcium sulfate, are presented in Section 3.5. Calcium carbonate and residual calcium sulfate were the main phases identified in the residues obtained for GGBS at 15 g/L (Fig. 4c) and 25 g/L (similar to Fig. 4c). However, the solid residue after the experiment at 50 g/L, showed the presence of calcium carbonate and sulfate together with hydrated magnesium sulfate and calcium phosphate (Fig. 4d). The presence of different solid residues obtained at 50 g/L compared to those obtained at 15 and 25 g/L is probably due to the pozzolan characteristics of GGBS, where calcium is able to react with silica in the presence of water to form calcium silicate hydrates (CSH). In the experiments described here, Ca is extracted from the parent material to produce $CaSO_4$ during the dissolution step. Consequently, in this work, the CSH group is decalcified, forming silica gel, which makes the solution dense and viscous as the S/L ratio is increased [27].

3.5. SEM–EDS of carbonated residues

SEM–EDS studies of the final solid residues obtained after experiments at 15 g/L were also carried out to characterize the structure and morphology of the carbonated particles.

Representative images obtained from the PS carbonated residue at 15 g/L are presented in Figs. 5a–c. The dispersed small particles

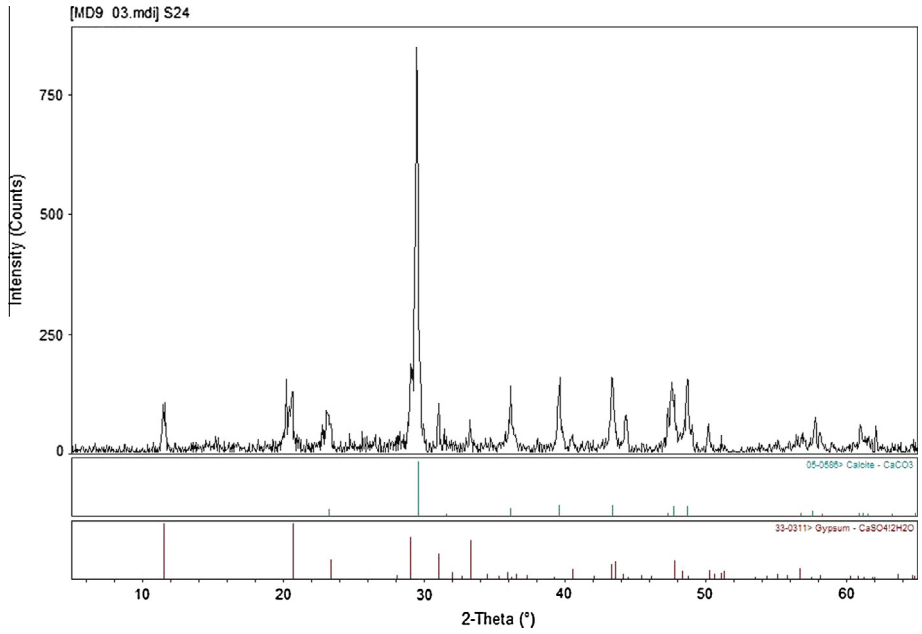

Fig. 4c. XRD diffractogram presenting crystalline phases detected in carbonated GGBS at 15 g/L.

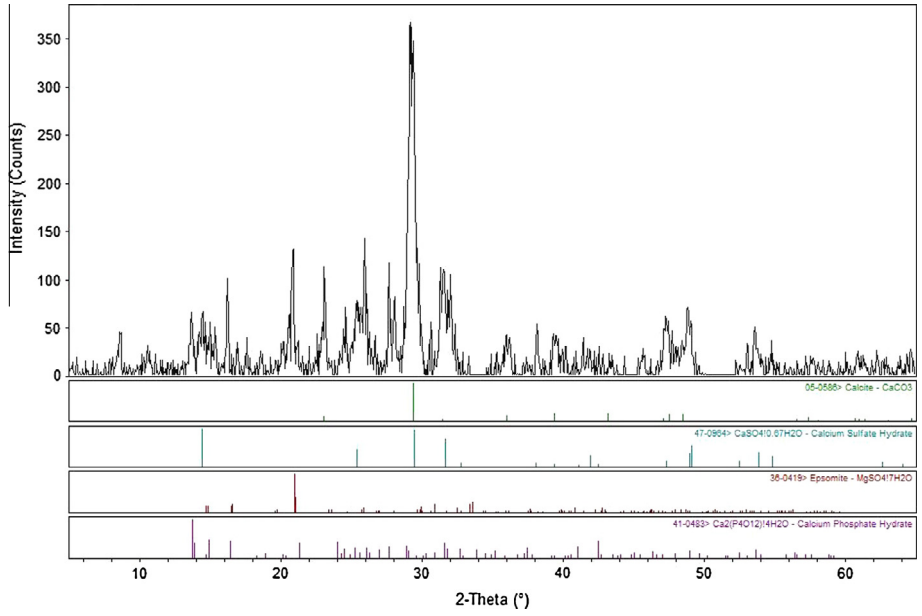

Fig. 4d. XRD diffractogram presenting crystalline phases detected in carbonated GGBS at 50 g/L.

seen in Fig. 5a and identified by the letter A, are precipitated calcium carbonate, magnified in Fig. 5b. The big particles in Fig. 5a (identified by letter B), are mainly residual calcium sulfate from the dissolution step and silica from the starting material. This is confirmed by the EDS studies, as shown in Fig. 5c where it can be seen that large calcium sulfate particles are plastered with small particles of calcium carbonate.

Following the characterization studies conducted using SEM–EDS, supported by XRD and XRF, the structure of the carbonated particles is discussed here. As the mineralization process consists of several consecutive steps (dissolution, pH adjustment and carbonation, Fig. 1), un-dissolved silica, which does not react during the dissolution step, forms a passive core as previously reported [6,28]. Layers of impurities precipitated from the pH adjustment step and calcium sulfate which was not converted into calcium carbonate during the following carbonation step are then likely to be formed, followed by the precipitation of calcium carbonate. This is consistent with previous studies conducted on carbonation of steel slag that showed a similar carbonated final product, where the core was formed by un-reacted silica and other un-dissolvable species, while the external layer consisted of precipitated calcium carbonate [20]. Furthermore, crystals precipitated during carbonation (Fig. 5b) seem very similar in shape and dimension to the ones found by Eloneva et al. in a previous work [29]. The final carbonated product, however, should be further treated to separate the different phases present and to obtain suitable valuable materials

(e.g. $CaCO_3$, SiO_2) [30]. Otherwise, the utilization of such carbonated materials could be restricted or limited to disposal in appropriate sites (e.g. mine/land reclamation projects).

The mineralization process developed by Wang and Maroto-Valer using serpentine reported that the rate limiting step of the dissolution reaction was the formation of a product layer of silica during the extraction of magnesium from serpentine [6]. That process is similar to the one described here, except that $MgSO_4$ formed during dissolution of serpentine dissolves, while $CaSO_4$ formed by the extraction of calcium from waste materials precipitates forming a layer of material on the original particles.

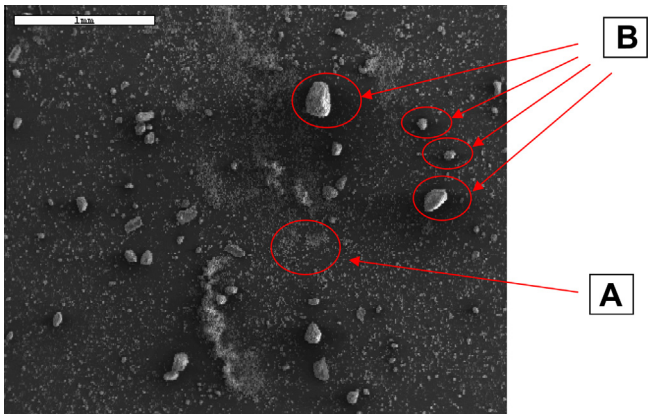

Fig. 5a. SEM image of PS carbonated residue at 15 g/L.

4. Conclusions

In this paper, a multi-step mineralization process was studied using three different waste materials (SS, PS and GGBS). The three samples have a high content of CaO (38%, 47% and 39% for SS, PS and GGBS, respectively) and, therefore, they have a good predisposition for mineral carbonation. XRD analyses showed that the mineral phases present in the parent materials were crystalline phases containing CaO for SS and PS while GGBS was mainly amorphous. The multi-step mineral carbonation process was investigated using three different S/L ratio (15–25–50 g/L) for all the three materials. The carbonation efficiencies increased with decreasing S/L ratio. Experiments at 15 g/L achieved 74%, 67% and 59% efficiency for SS, GGBS and PS, respectively. Wang and Maroto-Valer, using a similar process employing serpentine at 50 g/L, reached 25% efficiency which is lower than that of GGBS and SS at the same S/L ratio, and slightly above PS. This confirms that, in general, waste materials require less energy-intensive carbonation conditions, in comparison to mineral rocks. The solid residues from the carbonation step were analyzed using several techniques (XRF, XRD, SEM–EDS). XRF studies showed that reducing S/L ratio resulted in a decrease of SO_3 content. This is due to the production of $CaCO_3$ being higher when the S/L ratio is lower because of higher carbonation efficiency. XRD analyses found that the main phases identified in the carbonated samples were $CaCO_3$ and residual hydrated calcium sulfate ($CaSO_4{\cdot}2H_2O$).

The structure of the carbonated particles was also discussed. Silica from the raw samples did not dissolve and formed the particle core. $CaCO_3$ produced from the mineral carbonation process

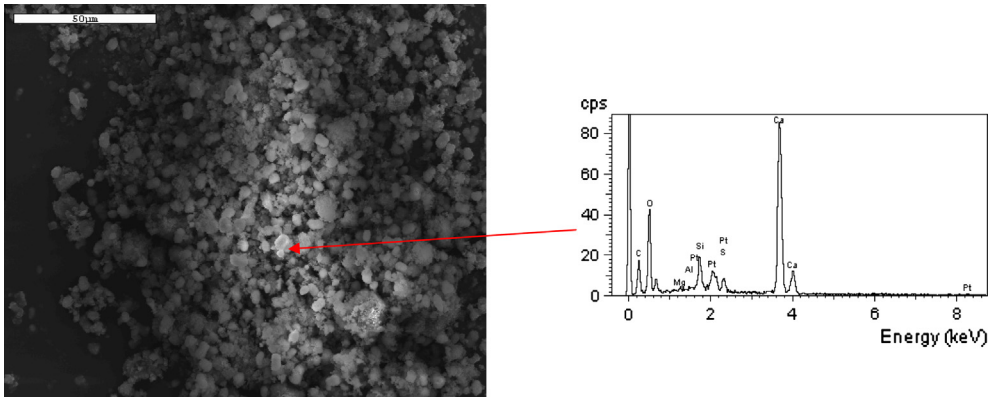

Fig. 5b. SEM image and EDS spectrograph of small particles of PS carbonated residue at 15 g/L.

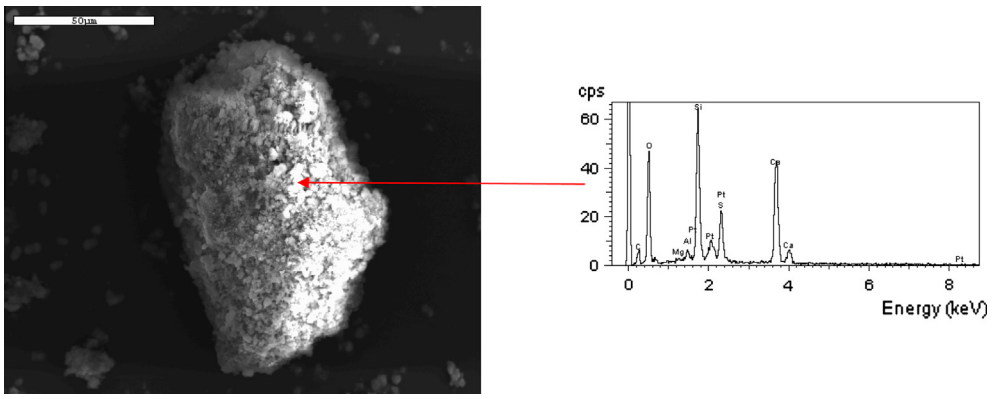

Fig. 5c. SEM image and EDS spectrograph of particles of PS carbonated residue at 15 g/L.

was deposited on the surface of the particles. $CaSO_4$ was the by-product left from incomplete carbonation reaction after dissolution and it is included in the core of the carbonated particles. $CaCO_3$ produced and deposited on the particles demonstrated that CO_2 was stored into these waste materials. However, by-products such as $CaSO_4$ and the original SiO_2 were also present, indicating that the final carbonated material should need further treatment to allow separation of the different phases to produce valuable final products (e.g. $CaCO_3$, SiO_2). A detailed kinetic evaluation and a continuously-operated bench-scale flow through unit are important areas for future investigation of the proposed process.

Acknowledgement

The financial support of the Centre for Innovation in Carbon Capture and Storage (CICCS) through EPSRC (EP/F012098/1 and EP/F012098/2) is gratefully acknowledged by the authors.

References

[1] IEA. CO_2 emissions from fuel consumption: 2011 highlights. Paris – France: IEA-international energy agency; 2011.
[2] Goldberg P, Chen Z, O'Connor W, Walters R. CO_2 mineral sequestration studies in US. National energy technology laboratory, department of enegy, US; 1998.
[3] IPCC. IPCC fourth assessment report: climate change. IPCC intergovernmental panel on climate change; 2007.
[4] EA. The climate is changing. EA environmental agency; 2005.
[5] IPCC. IPCC special report on carbon capture and storage. IPCC intergovernmental panel on climate change; 2005.
[6] Wang X, Maroto-Valer MM. Dissolution of serpentine using recyclable ammonium salts for CO_2 mineral carbonation. Fuel 2011;90:1229–37.
[7] Bobicki ER, Liu Q, Xu Z, Zeng H. Carbon capture and storage using alkaline industrial wastes. Prog Energy Combust Sci 2012;38:302–20.
[8] Wang X, Maroto-Valer MM. Integration of CO_2 capture and mineral carbonation by using recyclable ammonium salts. ChemSusChem 2011;4:1291–300.
[9] Zevenhoven R, Wiklund A, Fagerlund J, Eloneva S, In't Veen B, Geerlings H, et al. Carbonation of calcium-containing mineral and industrial by-products. Front Chem Eng Chin 2010;4:110–9.
[10] Baciocchi R, Costa G, Di Bartolomeo E, Polettini A, Pomi R. The effects of accelerated carbonation on CO_2 uptake and metal release from incineration APC residues. Waste Manage 2009;29:2994–3003.
[11] Baciocchi R, Costa G, Lategano E, Marini C, Polettini A, Pomi R, et al. Accelerated carbonation of different size fractions of bottom ash from RDF incineration. Waste Manage 2010;30:1310–7.
[12] Huntzinger DN, Gierke JS, Kawatra SK, Eisele TC, Sutter LL. Carbon dioxide sequestration in cement kiln dust through mineral carbonation. Environ Sci Technol 2009;43:1986–92.
[13] Monkman S, Shao Y. Assessing the carbonation behavior of cementitious materials. J Mater Civil Eng 2006;18:768–76.
[14] Huijgen WJJ, Ruijg GJ, Comans RNJ, Witkamp G-J. Energy consumption and net CO_2 sequestration of aqueous mineral carbonation. Ind Eng Chem Res 2006;45:9184–94.
[15] Costa G, Baciocchi R, Polettini A, Pomi R, Hills C, Carey P. Current status and perspectives of accelerated carbonation processes on municipal waste combustion residues. Environ Monit Assess 2007;135:55–75.
[16] Sanna A, Dri M, Hall MR, Maroto-Valer M. Waste materials for carbon capture and storage by mineralisation (CCSM) – a UK perspective. Appl Energy 2012;99:545–54.
[17] Olivier J, Janssens-Maenhout G, Peters J. Trends in global CO_2 emissions. The Hague – the Netherlands: PBL Netherlands environmental assessment agency; 2012.
[18] FisherScientific. Fisher scientific MSDS for calcium sulfate. Fisher scientific; 2013. <http://fscimage.fishersci.com/msds/97063.htm>.
[19] FisherScientific. Fisher Scientific MSDS for magnesium sulfate. Fisher scientific; 2013. <http://fscimage.fishersci.com/msds/13510.htm>.
[20] Back M, Kuehn M, Stanjek H, Peiffer S. Reactivity of alkaline lignite fly ashes towards CO_2 in water. Environ Sci Technol 2008;42:4520–6.
[21] Huijgen WJJ, Witkamp G-J, Comans RNJ. Mechanisms of aqueous wollastonite carbonation as a possible CO_2 sequestration process. Chem Eng Sci 2006;61:4242–51.
[22] Jo HY, Kim JH, Lee YJ, Lee M, Choh S-J. Evaluation of factors affecting mineral carbonation of CO_2 using coal fly ash in aqueous solutions under ambient conditions. Chem Eng J 2012;183:77–87.
[23] Wang X, Maroto-Valer MM. Optimization of carbon dioxide capture and storage with mineralisation using recyclable ammonium salts. Energy 2013;51:431–8.
[24] Huijgen W, Witkamp G, Comans R. Mineral CO_2 sequestration by steel slag carbonation. Environ Sci Technol 2005;39:9676–82.
[25] Yldirim I, Prezzi M. Chemical, mineralogical and morphological properties of steel slag. Adv Civil Eng 2011;2011:1–13.
[26] Back M, Kuehn M, Stanjek H, Peiffer S. Reactivity of alkaline lignite fly ashes towards CO_2 in water. Environ Sci Technol 2008:4520–6.
[27] Chen JJ, Thomas JJ, Jennings HM. Decalcification shrinkage of cement paste. Cement Concr Res 2006;36:801–9.
[28] Teir S, Revitzer H, Eloneva S, Fogelholm C-J, Zevenhoven R. Dissolution of natural serpentinite in mineral and organic acids. Int J Min Process 2007;83:36–46.
[29] Eloneva S, Teir S, Salminen J, Fogelholm C-J, Zevenhoven R. Steel converter slag as a raw material for precipitation of pure calcium carbonate. Ind Eng Chem Res 2008;47:7104–11.
[30] Sanna A, Hall MR, Maroto-Valer M. Post-processing pathways in carbon capture and storage by mineral carbonation (CCSM) towards the introduction of carbon neutral materials. Energy Environ Sci 2012;5:7781–96.